RSC Advances

PAPER

View Article Online
View Journal | View Issue

Cite this: *RSC Adv.*, 2026, **16**, 21639

From mononuclear to pyrazine-bridged dinuclear samarium(III) complexes: role of fluxidentate coordination in luminescent and thermal behavior

Vandana Aggarwal,[a] Devender Singh,[*ab] Swati Dalal,[a] Shri Bhagwan,[a] Sumit Kumar,[c] Rajender Singh Malik,[c] Parvin Kumar[d] and Jayant Sindhu[e]

Three Sm(III)-complexes featuring β-diketone ligand 4,4,4-trifluoro-1-thienyl-1,3-butadionate (TTBD) were studied for their potential as visible-light emitters. Utilizing pyz (pyrazine) as an ancillary ligand, two mononuclear compounds *i.e.* binary (SmA) and ternary (SmM) along with a dinuclear compound (SmD) were synthesized. Elemental (CHN), IR and NMR analyses confirmed that two complexes (SmA and SmM) are mononuclear with identical structural frameworks, whereas SmD forms a dinuclear species with pyrazine acting as a bridging ligand. The optical band gaps were measured from UV-vis absorption using Tauc's relation corresponding to HOMO–LUMO (Highest Occupied Molecular Orbital–Lowest Unoccupied Molecular Orbital) transitions. Photophysical investigations in solution phase using dichloromethane (DCM) solvent revealed characteristic emissions of Sm(III) ions under UV excitation, due to $^4G_{5/2} \rightarrow {}^6H_j$ (j = 5/2, 7/2, 9/2, 11/2) transitions in visible region. All complexes displayed intense luminescence with notably high lifetimes (0.063 ms), similar to the most efficient Sm(III)-based emitters reported. Radiative lifetimes and qualitative ligand-to-metal energy transfer (ET) efficiencies were deduced from time-resolved measurements, confirming that TTBD and pyz function effectively as sensitizing ligands. Colorimetric analysis based on emission spectra yielded CIE coordinates indicative of orange-red luminescence, typical of Sm(III) ions. Correlated color temperature (CCT) values further suggest their suitability as warm-light emitters. thermogravimetric analysis (TGA) revealed thermal stability up to ~224–231 °C, emphasizing their promise in thermally stable optoelectronic devices.

Received 19th January 2026
Accepted 20th April 2026

DOI: 10.1039/d6ra00472e

rsc.li/rsc-advances

1 Introduction

Lanthanide complexes, particularly those involving β-diketones and heterocyclic derivatives, have garnered noteworthy consideration in recent years owing to their promising utilizations in light conversion molecular devices (LCMDs).[1] The unique properties of lanthanide-based complexes like excellent optical characteristics and the potential for diverse functional applications, make them attractive candidates for advanced material design. The potential for these complexes to serve in a wide range of fields, from photonics[2] and sensors[3] to magnetics,[4] continues to drive extensive research and development. Furthermore, the ability to tune these materials by changing their chemical structure offers exciting possibilities for the next generation devices. Lanthanide ions exhibit intricate electronic configurations due to presence of diffused 4f orbitals leads to a unique set of chemical and spectroscopic properties that distinguish lanthanide complexes from those of transition metals. Most lanthanide ions stabilize in the +3 oxidation state, in which the 4f orbitals are relatively open, allowing the preparation of complexes with different ligands. β-diketones are particularly effective ligands for lanthanide complexes.[5] These ligands provide a strong coordination sphere and also serve as energy transfer units, further increasing the luminescence of resulting complexes.

Particularly, β-diketones can facilitate energy transfer from ligands to metal ions, a phenomenon often referred as the antenna effect.[6] This effect is especially relevant in the context of lanthanide luminescence, where 4f–4f transitions of Ln(III) ions are often parity-forbidden and thus inefficient. By absorbing UV light, ligand can excite its own electronic states and transfer energy to the metal center, enabling the lanthanide ion to undergo a highly efficient luminescent emission. This mechanism is key to the performance of lanthanide complexes in various optoelectronic applications. The emission characteristics of lanthanide complexes are another key

[a]*Department of Chemistry, Maharshi Dayanand University, Rohtak-124001, Haryana, India. E-mail: devjakhar@gmail.com*
[b]*Department of Chemistry, Lovely Professional University, Phagwara, Jalandhar, Punjab, 14441, India*
[c]*Department of Chemistry, DCR University of Science & Technology, Murthal-131039, Haryana, India*
[d]*Department of Chemistry, Kurukshetra University, Kurukshetra-136119, Haryana, India*
[e]*Department of Chemistry, COBS&H, CCS Haryana Agricultural University, Hisar-125004, Haryana, India*

feature that makes them highly desirable for use in devices such as sensors and organic light-emitting diodes (OLEDs). Long-lived, sharp emission bands characteristic of Ln(III) ions are a result of electronic transitions within 4f orbitals of metal center.[7] These emission wavelengths can be tailored by selecting different lanthanide ions, allowing for the generation of materials with specific emissive properties. For example, complexes of Sm(III) and Tb(III) ions are particularly noted for their intense orange-red and green emissions, respectively, which are highly desirable for display and lighting technologies. Emission intensity and lifetime of these complexes can be further optimized by carefully selecting the ligands that sensitize the metal ion based luminescence. Ideally, the triplet state (T_1) of ligand should closely match excited state energy of Ln(III) ion, facilitating efficient energy transfer and resulting in enhanced emission intensity and prolonged luminescence lifetimes.[8]

Recently, there has been growing interest in dinuclear lanthanide complexes, which consist of two metal centers bridged by ligands. These complexes have been studied for a variety of reasons, including their potential to improve the luminescence of mononuclear lanthanide complexes. The combination of two metal centers may offer synergistic effects, such as improved luminescence intensity or modified emission characteristics.[9] Additionally, dinuclear lanthanide complexes provide an opportunity to explore magnetic interactions among metal centers, which may be useful for improvement of advanced tools with tailored magnetic features.[10] The bridging ligands used in these complexes can vary widely, but polyazine-based ligands are particularly notable for their ability to bridge lanthanide ions while also facilitating energy transfer. Ligands like dpp (2,3-bis-dipyridylpyrazine), bpm (2,2′-bipyrimidine), pyz (pyrazine) and tpp (tetra-2-pyridylpyrazine) have been successfully employed to form stable and luminescent lanthanide complexes.[11] In this context, a bridged samarium complex $[Sm_2(TFPB)_6(pyz)]$; SmD along with its monometallic $[Sm(TTBD)_3(pyz)_2]$; SmM and binary conjugate $[Sm(TTBD)_3(H_2O)_2]$; SmA are synthesized, involving a heteroaryl 1,3-diketone (4,4,4-trifluoro-1-(2-thienyl)-1,3-butanedione, TTBD) and polyazine (pyz, pyrazine) ligand. The unique electronic properties of samarium, coupled with its ability to form stable and luminescent complexes is exploited to generate complexes that may act as ideal candidates for the formation of innovative materials in areas including optoelectronics, photonics and biomedical diagnostics.

2 Material and techniques

Commercially available chemicals *i.e.* $SmCl_3 \cdot 6H_2O$ (99.99%), pyz and TTBD were sourced from Sigma-Aldrich and used as received without any additional purification. Used solvents, ethanol and hexane, were AR/SR and the base (25% ammonia solution) was obtained from ResearchLab. C, H and N content of prepared complexes was evaluated on PerkinElmer 2400 Elemental Analyzer. IR Transmittance profiles of SmA–SmD were noted in the 400 to 4000 cm^{-1} range utilizing a PerkinElmer 5700 FTIR Spectrometer. Proton magnetic resonance (PMR) data were attained in DMSO-d_6 on a Bruker Avance II NMR spectrometer working at 400 MHz. Electronic absorption profiles of TTBD and prepared complexes were collected in DCM solvent (conc.: 10^{-5} M) using the Shimadzu Ultima 2450 spectrophotometer. Photoluminescence (PL) excitation and emission profiles of complexes in solution phase were taken on a Horiba Jobin FL-3-11 YVON Fluorolog spectrophotometer. The absorption spectra are presented in normalized form for clarity. The absorbance at the excitation wavelength ($\lambda_{ex} = 342$ nm) was measured for each sample and considered during analysis (absorbance ~1.66, 1.09 and 1.05 a.u. for SmD, SmM and SmA, respectively). All emission spectra were recorded under identical instrumental condition and intensity comparisons were made with consideration of absorbance at λ_{ex}. Time-resolved spectral profiles were taken on F-7000 FL Spectrophotometer with 20 ms scan rate. Thermogravimetric (TG) curves were noted on Hitachi STA-7300 thermal analyser at 10 °C min^{-1} heating rate in inert atmosphere.

3 Synthesis

3.1 $[Sm(TTBD)_3(H_2O)_2]$

5 mL ethanolic solution of 2.16 mmol of $SmCl_3 \cdot 6H_2O$ and an alcoholic solution of 6.48 mmol of TTBD were prepared separately. To the TTBD solution, NH_4OH solution was added dropwise (6.48 mmol) to convert it into its ammonium salt. Then, 5 mL of an aqueous solution containing metal salt was added dropwise to the resulting TTBD solution under stirring at room temperature, adjusting the pH to ~7 by using NH_4OH solution. Reaction mixture was then heated at 65 °C to form off-white solid. It was then filtered, washed with distilled water and dried (Fig. 1).[12,13]

3.2 $[Sm(TTBD)_3(pyz)_2]$

An *in situ* method was used to form this complex.[14–16] Fig. 2 illustrates the synthesis of $[Sm(TTBD)_3(pyz)_2]$. Initially, 6.48 mmol of 25% aqueous ammonia solution was added dropwise to 5 mL of an ethanolic solution of TTBD (6.48 mmol) to facilitate deprotonation of the ligand. The resulting mixture was allowed to stand for several hours to ensure completion of the reaction, resulting in the formation of $NH_4(TTBD)$, the ammonium salt of diketone. This solution was then combined with 5 mL ethanolic $SmCl_3 \cdot 6H_2O$ (2.16 mmol) and pyz (4.32 mmol) solution. Molar ratio between $SmCl_3 \cdot 6H_2O$, TTBD and pyz were kept at 1 : 3 : 2. Mixture was stirred overnight at RT under nearly neutral pH (~7) conditions. During this stirring process, a cream colored precipitate formed, which was then filtered out. Filtrate was concentrated and left for slow evaporation at RT. Resulting precipitates were washed with ethanol and hexane and then dried.

3.3 $[(Sm(TTBD)_3)_2\ pyz]$

In a similar reaction, the complex $[Sm(TTBD)_3(H_2O)_2]$ reacted with pyrazine in a 2 : 1 molar ratio. Following slow solvent evaporation over 24 hours, a new seven coordinated dinuclear

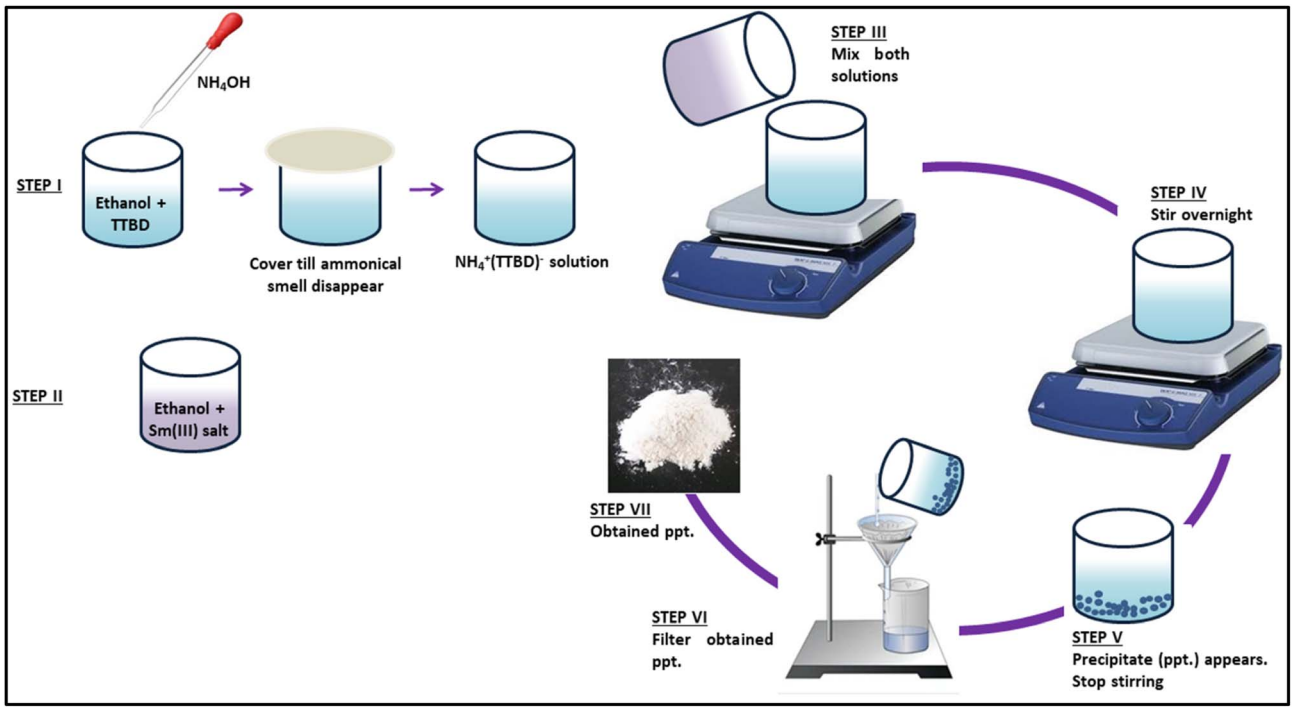

Fig. 1 Synthesis pathway for SmA.

complex was isolated (Fig. 3).[17,18] The confirmation that both nitrogen atoms of pyz are involved in bonding, with pyz acting as a spacer to bind two $Sm(TTBD)_3$ groups was made *via* CHN, IR and proton NMR analysis. Moreover, their PL properties have further been noted.

4 Results and discussions

4.1 CHN study

The mononuclear complex with H_2O was off-white solid (SmA), while with pyz was cream (SmM) in color. The elemental

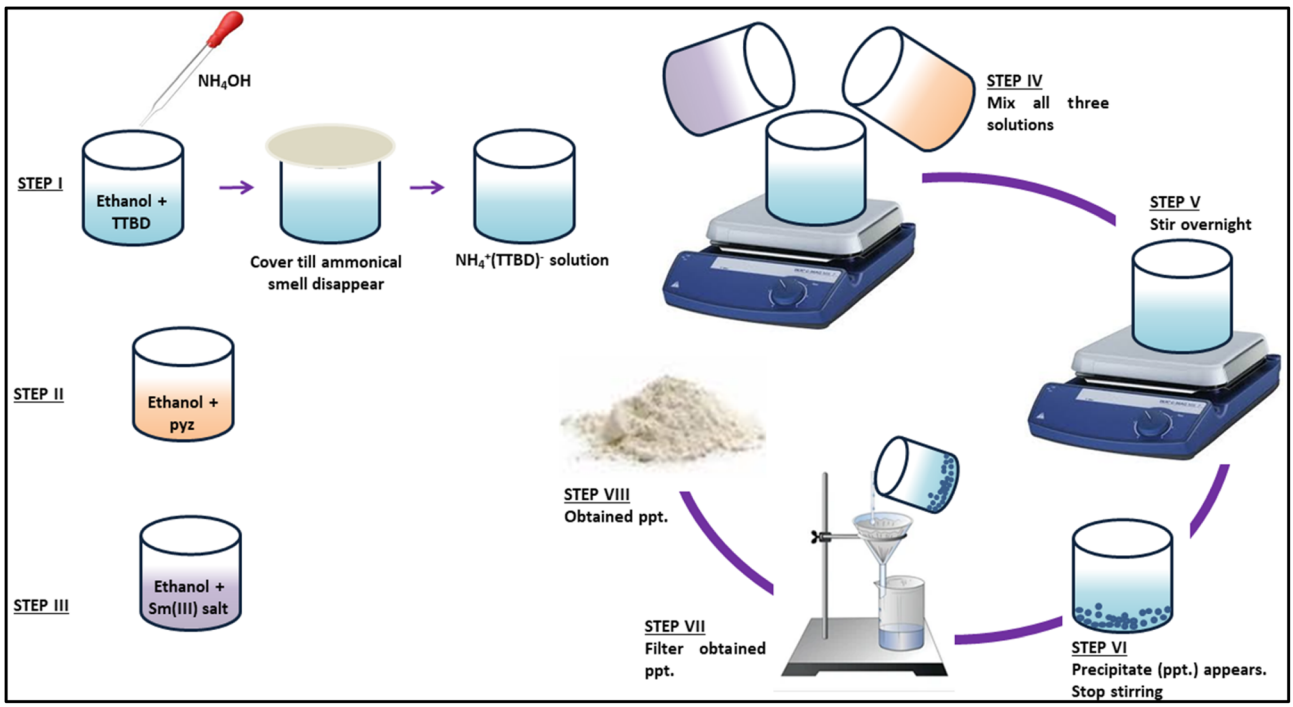

Fig. 2 Synthesis pathway for SmM.

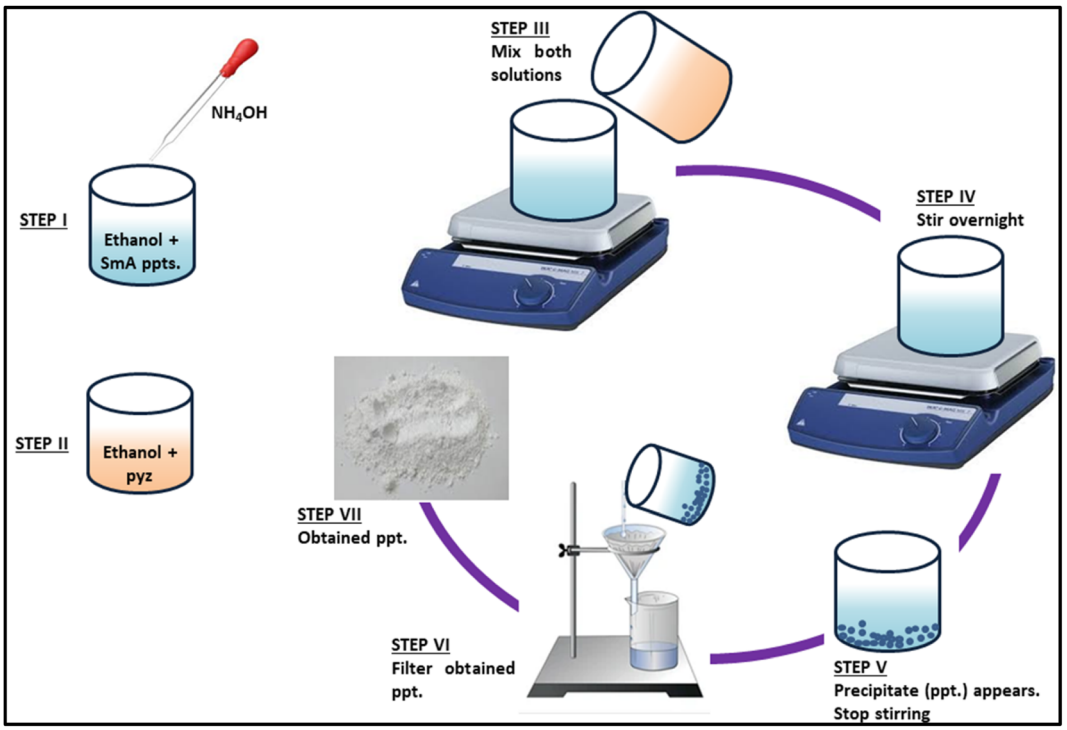

Fig. 3 Synthesis pathway for SmD.

analysis results suggested empirical formulations which matched the theoretical data, by minimal deviations, confirming accuracy of data. Table 1 presents experimental (E) and theoretical (T) % compositions of C, H and N for SmA–SmD, along with proposed and abbreviated formulations. Dinuclear complex was obtained as white solid with high hygroscopicity (approximately 30% water content). Dinuclear complexes exhibit greater solubility in DMSO compared to their mononuclear analogues. The incorporation of an additional $Ln(TTBD)_3$ unit in the dinuclear complex seems to enhance its solubility.[19]

Table 2 IR data (in cm^{-1}) of free sensitizers with SmA–SmD

Complex	TTBD	pyz	SmA	SmM	SmD
$\nu_{(Sm-O)}$	—	—	452	465	459
$\nu_{(Sm-N)}$	—	—	—	584	584
$\nu_{(C-F)}$	—	—	1133, 1193	1133, 1193	1133, 1193
$\nu_{(C-N)}$	—	—	—	1358	1372
$\nu_{(C=C)}$	—	1457	1458	1458, 1511	1471, 1498
$\nu_{(C=N)}$	—	—	—	1544	1537
$\nu_{(C=O)}$	1655	—	1610	1604	1590
$\nu_{(=CH)}$	—	—	2933	2847	2927

4.2 IR study

Infrared spectroscopy was used to assign the bands of the free sensitizers and to identify changes related to coordination with the metal ions in mononuclear complexes. Primary peaks for uncoordinated and coordinated sensitizers are summarized in Table 2. Additionally, the FTIR spectra of SmA–SmD have been provided in SI as Fig. S1–S3. The complexes displayed both blue and red shifts in their bands compared to the free ligands, showing coordination with trivalent samarium ions. Notably, transitions near 400 cm^{-1} were attributed to Sm–N (stronger intensity) and Sm–O (weaker intensity) stretches.[20] The appearance of these stretches further affirmed the aforementioned coordination in the complexes. Each infrared spectrum showed a considerable change in stretching vibration of C=O band from 1655 cm^{-1} in uncoordinated ligand to lower wavenumber in prepared complex, proposing coordination to metal ion.[21] The IR spectra revealed that the major carbonyl stretch in $Sm(TTBD)_3 \cdot 2H_2O$ was ~1610 cm^{-1}, shifting to 1604 cm^{-1} for

Table 1 % CHN content (E and T) in SmA–SmD

Complex	Color	C_E (T)	H_E (T)	N_E (T)	Formula
SmA	Off-white	33.87 (33.92)	1.99 (1.90)	—	$C_{24}H_{16}SmF_9O_8S_3$
SmM	Cream	39.43 (39.46)	1.95 (2.07)	5.66 (5.75)	$C_{32}H_{20}SmF_9N_4O_6S_3$
SmD	White	36.46 (36.57)	1.76 (1.65)	1.57 (1.64)	$C_{52}H_{28}Sm_2F_{18}N_2O_{12}S_6$

Table 3 PMR shifts of prepared complexes in ppm

Complex	Peaks due to TTBD	Peaks due to pyz
Uncoordinated	14.9 (1H), 7.84 (1H), 7.60 (1H), 7.20 (1H), 6.45 (1H)	8.50 (4H)
SmA	2.96 (3H),7.17–7.29 (6H), 7.86 (3H)	—
SmM	3.05 (3H), 7.21–7.32 (6H), 8.14 (3H)	7.86 (4H), 8.65 (4H)
SmD	2.88 (6H), 7.30–7.56 (18H)	8.10 (4H)

$[Sm(TTBD)_3(pyz)]$ and 1590 cm^{-1} for $[Sm_2(TTBD)_6(pyz)]$. These shifts suggest that the β-diketonate ($Sm(TTBD)_3$) complex coordinated with ligands (pyz). The infrared spectra of synthesized complexes exhibited vibration modes at CH_2 (2900 cm^{-1}), C=C (1460–1500 cm^{-1}), C=N (1540 cm^{-1}) and C–N (1360 cm^{-1}).[22,23] Additionally, SmA revealed a strong band in 1645–1623 cm^{-1} region, likely corresponding to $\delta_{(OH)}$ vibration of H_2O.[24] Additionally, the C=N bond frequency shifted from 1605 cm^{-1} (pyz) to 1544 and 1537 cm^{-1} in the SmM and SmD, respectively. These changes support the coordination of N-atom of sensitizing moiety with Sm(III) ion (Table 2). Furthermore, the $\nu_s(CF_3)$ band in TTBD appeared at ~1139 cm^{-1} in the complexes, indicating that Sm(III) ions coordinate with TTBD. Major signature peaks of free pyz were masked by the strong peaks due to TTBD in SmM and SmD spectra. However, a peak ~1457 cm^{-1} in uncoordinated pyz shifts to ~1458–1511 cm^{-1} upon coordination. In SmM, coordination through a single N-atom (of pyz) reduces its symmetry, leading to the presence of a new peak in the 930–1010 cm^{-1} range. A distinctive band ~944 cm^{-1} in SmM, absent in SmD, further confirms monodentate coordination of pyz. Furthermore, the appearance of a typical O–H stretching

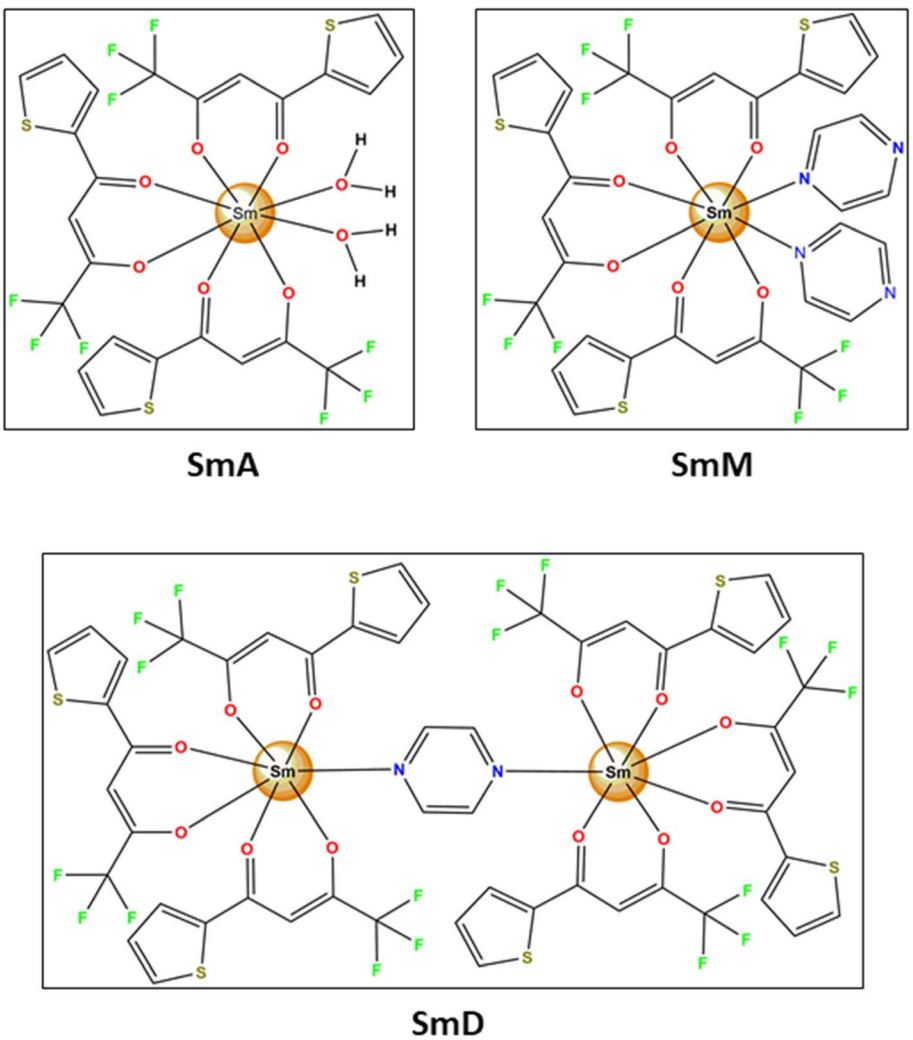

Fig. 4 Structure of prepared complexes.

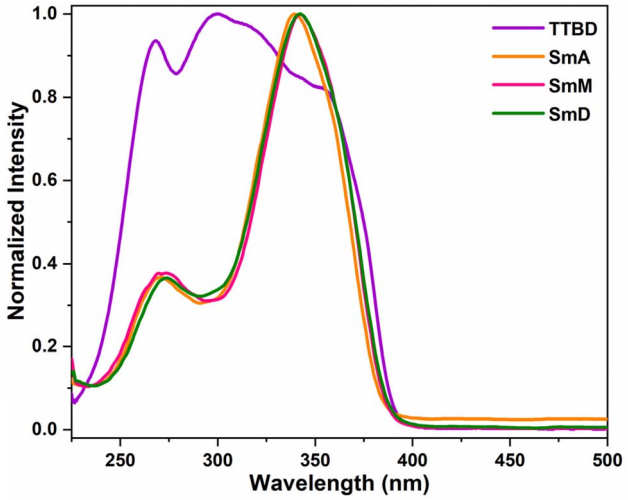

Fig. 5 Normalized electronic absorption profiles of TTBD and prepared complexes.

Table 4 Some optical parameters of prepared complexes

Complex	λ_{abs}	E_g	λ_{ex}	λ_{em}	R_{Sm}	Lifetime (ms)
SmA	270, 339	3.319	274, 375	646	12.51	0.004
SmM	271, 342	3.291	280, 368	647	9.77	0.058
SmD	273, 342	3.287	283, 369	647	9.08	0.063

band ~3400 cm^{-1} in SmA suggests the presence of coordinated water, while the lack of this band in SmM and SmD confirms the absence of water in these complexes.

4.3 Proton nuclear magnetic resonance (^{1}H-NMR) study

NMR spectroscopy confirmed the synthesis of the desired dinuclear complex. The NMR spectrum of free pyrazine shows single peak at 8.5 ppm.[25] While TTBD displays peaks due to thiophene ring at 7.84, 7.60, 7.20 ppm, at 14.9 ppm for O–H proton and at 6.45 ppm for methine proton as a sharp singlet.[26] The assigned ^{1}H NMR proton resonances corresponding to the ligand framework of the complexes are summarized in Table 3. Additionally, the proton NMR spectra of prepared complexes have been provided in SI as Fig. S4–S6. The signals of pyz coordinated in SmM are significantly shifted compared to those of the free sensitizer. Intensity ratio among methine (TTBD) and pyz signals approves that Sm(III) coordinates with two pyz moieties and three TTBD units, forming an eight coordinated structure.

The NMR spectrum of SmD complex supports a pyrazine-bridged dinuclear structure exhibiting three signals, two from TTBD and one from pyrazine. These peaks support the existence of two Sm(TTBD)$_3$ units and a pyz moiety in the complex. Furthermore, a strong peak at 2.88 ppm, integrating for six protons, corresponds to the =CH protons of TTBD attached to two Sm(III) ions. In the aromatic region, a sharp singlet at 8.10 ppm integrating for four protons is consigned to the pyz protons. Notably, this resonance is shifted downfield in the Sm–Sm complex relative to free pyz, indicating deshielding of the ring protons as a consequence of coordination with the metal ions. It is noteworthy that when pyz coordinates *via* single N-atom, it typically shows two resonances of comparable intensity, but here, single sharp resonance is observed, confirming the symmetric bridging of pyz between the two Sm(TTBD)$_3$ entities. Moreover, these complexes exhibited a shift in the resonances of pyz and TTBD to both sides *i.e.* upfield and downfield. These opposite directional shifts within a given complex suggest that these shifts are dipolar in nature.[27] It is most prominent for the protons closer to metal ion, indicating that this dipolar shift is influenced by the distance among metal ion and the resonating nucleus which decreases as the proton moves farther from the metal ion. Moreover, SmA exhibits two signals in PMR spectrum due to diketonic moiety, a singlet due to methine proton with a multiplet due to thienyl protons.

The combined spectroscopic analyses provide consistent evidence for the coordination environment of the synthesized complexes. Elemental analysis confirms the proposed stoichiometry, while FTIR spectroscopy reveals characteristic shifts in the β-diketonate carbonyl stretching frequencies, indicating coordination of the ligand to the Sm(III) center. The NMR spectra further support the ligand environment around the metal ion. Taken together, these results support the formation of mononuclear SmA and SmM complexes, whereas the incorporation of pyrazine as a bridging ligand leads to the formation of the dinuclear SmD complex with a modified coordination environment. Based on these analyses, the probable structure of complexes is deduced and presented in Fig. 4. In the mononuclear complexes, the Sm(III) ion adopts an octacoordinated geometry formed by the chelating β-diketonate ligands and auxiliary donor atoms. In contrast, in the dinuclear complex the pyrazine ligand acts as a bridging ligand between two Sm(III) centers through its N-atoms. This bridging coordination imposes geometric constraints and limits the number of ligands that can coordinate around each metal center, resulting in a stable heptacoordinated environment for the Sm(III) ions. Such variations in coordination number are commonly observed in lanthanide complexes due to the flexible coordination preferences of Ln(III) ions.

4.4 UV analysis

Electronic spectrum of free TTBD displays two highly intense absorptions in 225–280 nm and 280–400 nm region due to strong $^1\pi$–π^* transition of ligands, exhibiting high molar absorption coefficients (ε, ~10^4 L mol^{-1} cm^{-1} for TTBD and ~10^3 L mol^{-1} cm^{-1} for pyz), which indicate efficient light harvesting ability of the ligands.[28] Maxima of these singlet-to-singlet electronic excitations appear ~268 and 299 nm in DCM. The spectra show strong light absorbing properties of ligands. Electronic profiles of complexes show two strong bands at 270, 339 nm (SmA); 271, 342 nm (SmM) and 273, 342 nm (SmD), which is the combined absorption of both ligands (Fig. 5). This absorption band is red-shifted by ~43 nm for TTBD (from 299 to 342 nm), indicating coordination of the sensitizers to metal ions. Coordination of metal center to ligand stabilizes the π^* orbitals of TTBD, resulting in absorption shifts

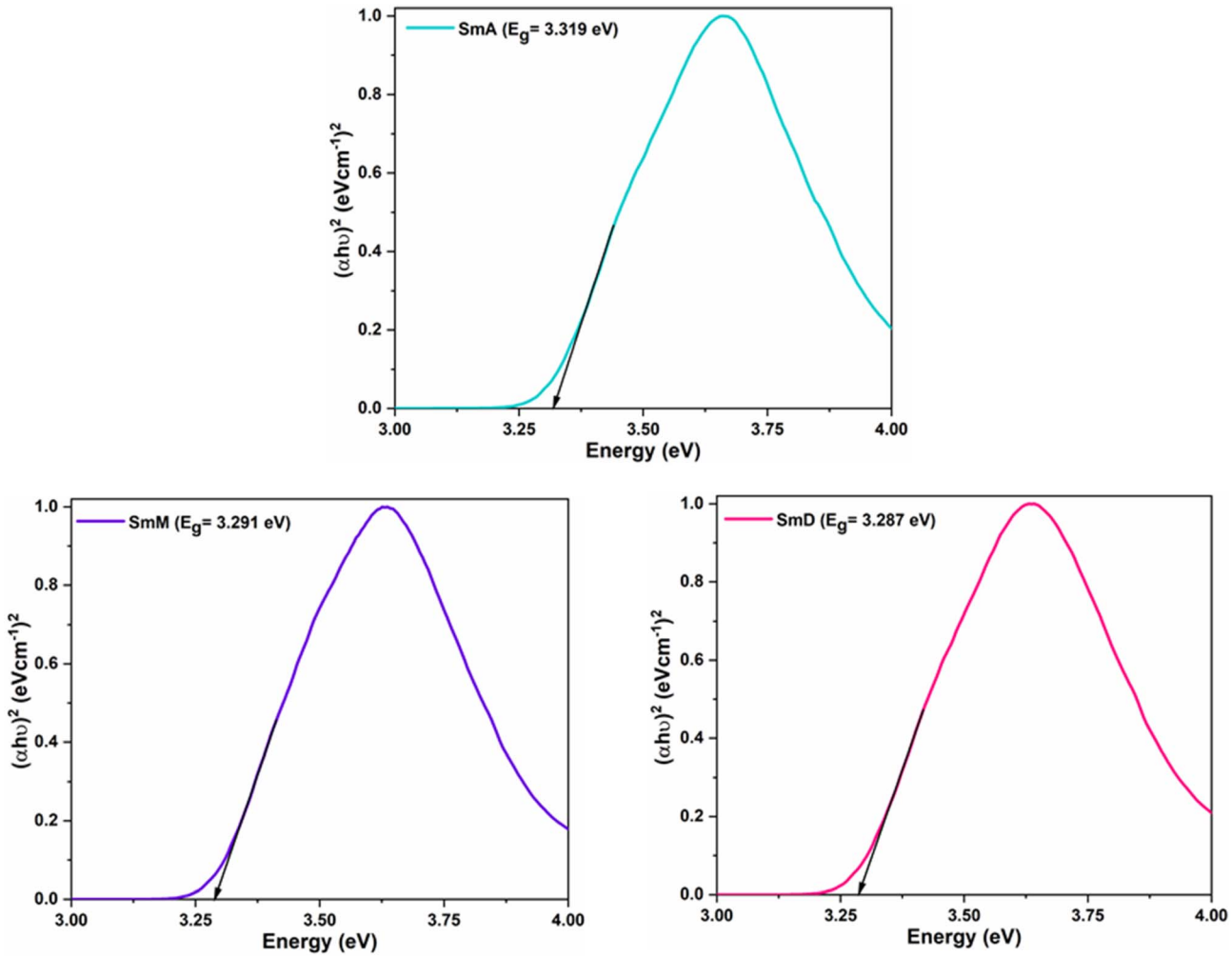

Fig. 6 Bandgap profiles of prepared complexes.

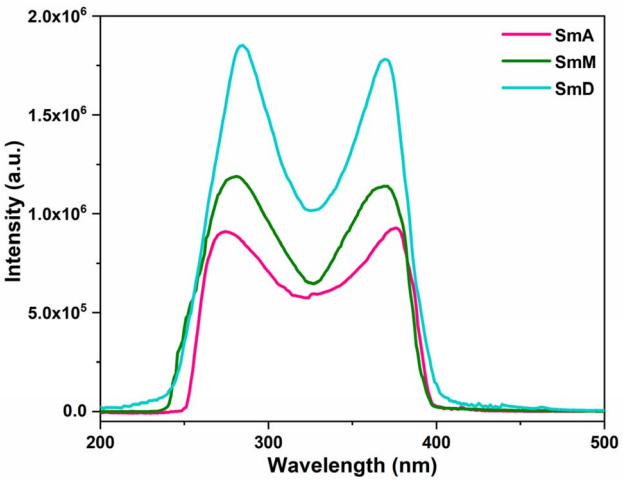

Fig. 7 Excitation profiles of prepared complexes in DCM.

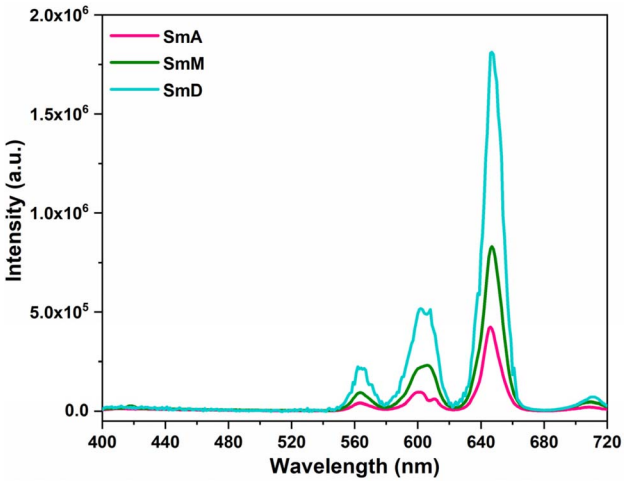

Fig. 8 Emission profiles of prepared complexes in DCM.

to lower energy. Table 4 consists of the absorption maxima for bands attributed to π, n → π* transitions for the prepared complexes. No transitions are noticed in visible region, affirming the non-existence of metal-to-ligand charge transfer transitions. Spectrum of $Sm(TTBD)_3$ is indistinguishable to that of the bridged dinuclear Sm(III) complex but slight red-shifted

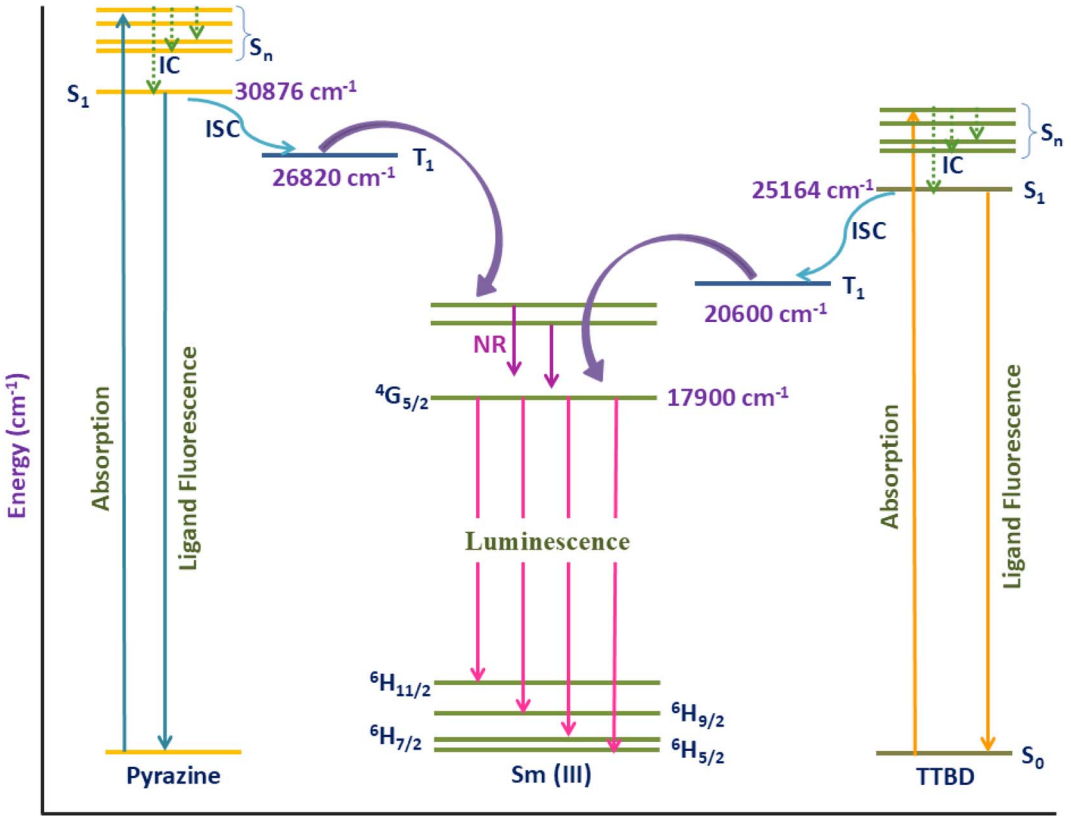

Fig. 9 Schematic diagram of probable energy transfer occurring in SmA–SmD. Here, IC = internal conversion, ISC = intersystem crossing, S_n = higher singlet states, NR = non-radiative transition.

Table 5 T_1 energy with their energy gap with emitting level of central ion

Compound	Energy (cm^{-1})
E_{pyz}	26 820
E_{TTBD}	20 600
$E_{Sm(III)}$	17 699
$\Delta E_{TTBD\text{-}Sm(III)}$	2901
$\Delta E_{Pyz\text{-}Sm(III)}$	9121

suggested that when pyz coordinates with two $Sm(TTBD)_3$ entities, π*-orbitals are stabilized to lower energy. This stabilization of the bridging π* orbitals upon coordination with Ln(III) ions is also detected with dipyridyl tetrazine bridging ligand.[29]

4.4.1 Band gap determination. Optical bandgap (E_g) was determined from electronic absorption data by applying Tauc's relation,[30] eqn (1), where h is Planck constant, d is optical path, ν is incident radiation frequency, A is absorbance, α is correction to absorbance and n is either 1/2 or 2 depending upon allowed direct transitions and forbidden transitions character, respectively. E_g was attained by extrapolation of $(\alpha h\nu)^2$ v/s energy ($h\nu$) spectrum.[31]

$$\alpha h\nu = A(h\nu - E_g)^n \quad (1)$$

Fig. 6 depicts their obtained curves and Table 4 constitutes the quantitative E_g data found to be ~3.3 eV, which affirms the semiconducting properties possessed by these complexes and may possibly hold potential for photonic applications.[32]

4.5 Photoluminescence (PL) properties

4.5.1 PL excitation and emission. PL features of the prepared complexes were explored at RT. Their excitation profiles (Fig. 7) were noted by monitoring hypersensitive emission transition $^4G_{5/2} \rightarrow {}^6H_{9/2}$ at 647 nm[33] within a selected wavelength range corresponding to the ligand absorption region responsible for sensitizing the Sm(III) emission. These spectra are characterized by a broad and intense band ranging from 237 to 400 nm, with maximum excitation wavelengths at 274 and 375 nm for SmA, 280 and 368 nm for SmM and 283 and 369 nm for SmD. These bands are consigned to the excitation of the organic sensitizers.[34] The excitation profiles of all the prepared complexes exhibit similar patterns because the TTBD ligand serves as the principal sensitizer responsible for absorbing excitation energy and transferring it to the Sm(III) center. Consequently, the overall excitation patterns remain comparable despite variations in the auxiliary ligand environment. However, differences in intensity are observed, which may result from variations in coordination modes and the number of sensitizers involved. Moreover, predominance of intraligand $S_0 \rightarrow S_1$ transitions proposes an efficient energy

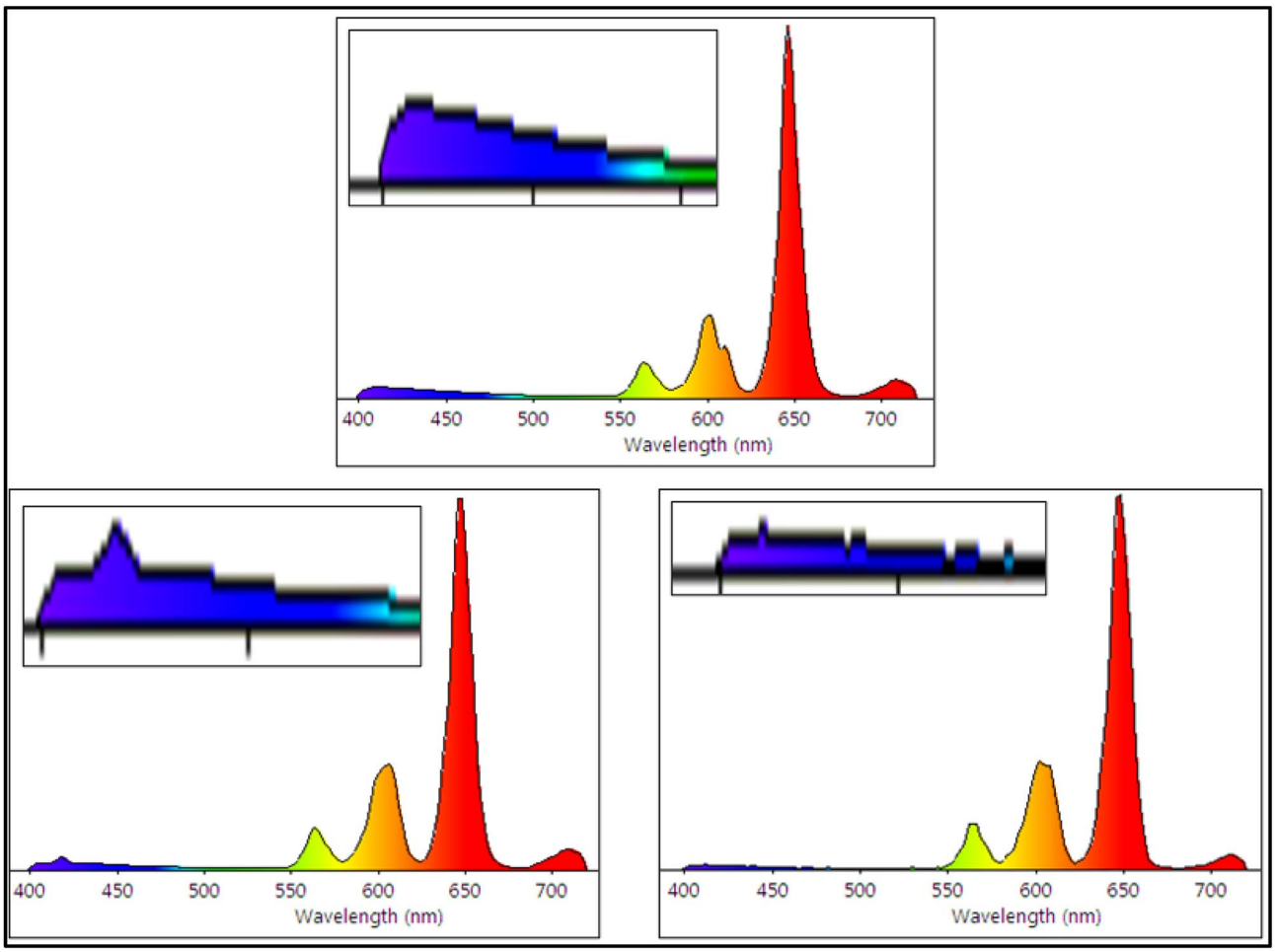

Fig. 10 Color contribution of each peak towards emissive color in SmA–SmD.

Table 6 β-value (%) for prepared complexes

	Branching ratio			
Complex	$\Delta J = 0$	$\Delta J = 1$	$\Delta J = 2$	$\Delta J = 3$
SmA	5.68	18.27	71.11	4.92
SmM	6.63	23.74	64.78	4.52
SmD	7.20	24.66	65.43	2.69

transfer from sensitizers towards the Sm(III) ion.[35] This conclusion is supported by the observation that the emission spectra (mentioned later, Fig. 8) are dominated by the characteristic Sm(III) f–f transitions, while only very weak ligand-centered emission is observed in the blue region.

The PL emission spectra (Fig. 8) were obtained using excitation wavelengths (λ_{ex}) derived from the excitation spectra. Emission peaks observed ~563, 603, 647 and 710 nm correspond to transitions: (i) $^4G_{5/2} \rightarrow {}^6H_{5/2}$, (ii) $^4G_{5/2} \rightarrow {}^6H_{7/2}$, (iii) $^4G_{5/2} \rightarrow {}^6H_{9/2}$ and (iv) $^4G_{5/2} \rightarrow {}^6H_{11/2}$, respectively.[36] First peak ($\Delta J = 0$) is magnetic dipole (MD) and is unaffected by coordination environment of Sm(III) ion, making it suitable as a ref. 37. Second transition ($\Delta J = 1$), although allowed as a magnetic dipole transition, has a significant electric dipole (ED) component and is often considered a mix of both.[38] The third transition ($\Delta J = 2$) is a purely electric dipole and is highly sensitive to changes in samarium coordination environment. Fourth transition ($\Delta J = 3$) is forbidden and exhibits low intensity. Among these, the hypersensitive $\Delta J = 2$ transition dominates the emission spectra and reflects the asymmetry about the Sm(III) center. Intensity trend follows: $\Delta J = 2 > 1 > 0 > 3$. Intensity ratio (R_{Sm}) of ED to MD transition serves as an indicator of asymmetry in the local environment of Sm(III) ion. R_{Sm} values for complexes in DCM are found to be: 12.51 (SmA) > 9.77 (SmM) > 9.08 (SmD), suggesting a progressively more asymmetric environment around the samarium ion.[39] Although all complexes exhibit similar spectral shapes with overlapping features, PL intensity of SmD is manifolds higher than that of SmM. This enhanced emission is likely due to higher quantity of TTBD groups coordinated to Sm(III) ion in SmD, enabling more efficient energy transfer. In contrast, SmA shows diminished luminescence due to the occurrence of high energy O–H oscillators' which perform as quenching agents.[40]

In addition to metal centered peaks, a weak ligand centered emission band in the range of ~400–470 nm is noticed for SmA, which can be credited to non-radiative relaxation paths

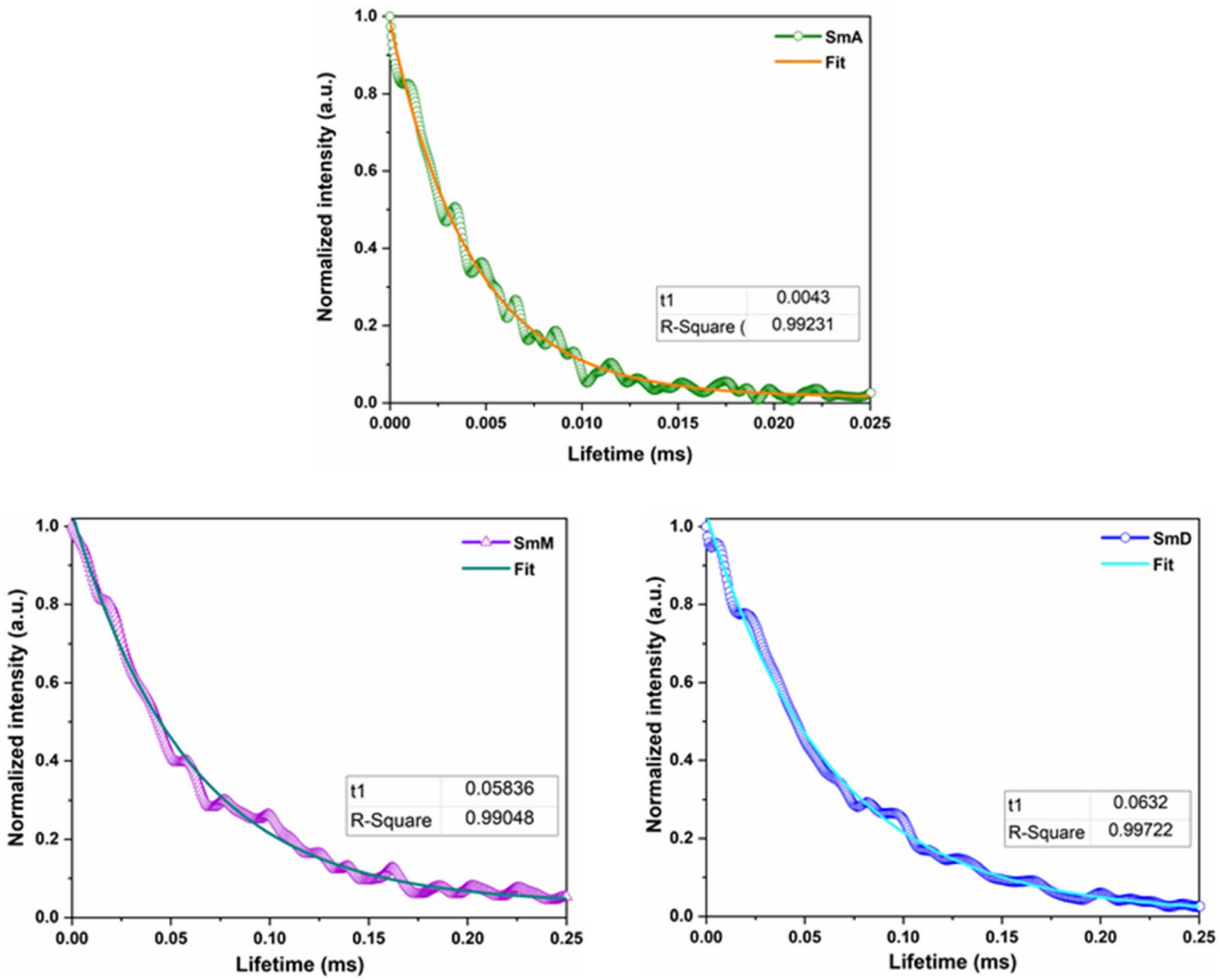

Fig. 11 Decay lifetime profiles of SmA–SmD.

introduced by coordinated solvent molecules. This results in SmA exhibiting the lowest emission intensity among the three complexes. Similarly, SmM also shows a minimal ligand-based emission band, likely due to the large energy gap among emissive state of the Sm(III) ion and donor level of pyz. Although SmD contains the same sensitizers, its emission intensity is

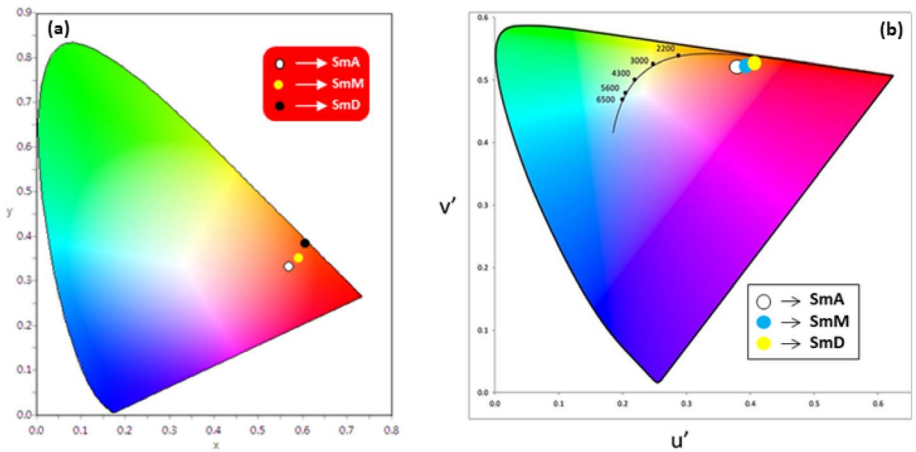

Fig. 12 (a) CIE 1931 (*x*, *y*) (b) 1976 (*u*′, *v*′) plot of SmA–SmD.

Table 7 (x, y) and (u', v') values of prepared complexes

Complex	SmA	SmM	SmD
x, y	0.568, 0.332	0.589, 0.344	0.610, 0.358
u', v'	0.388, 0.511	0.395, 0.520	0.401, 0.530
CCT (K)	1290	1253	1223

significantly higher than that of SmM. This enhancement can be attributed to lower number of pyz sensitizers coordinated to metal ion (one in SmD *versus* two in SmM). These observations further confirm that TTBD acts as a more efficient sensitizer for Sm(III) ion than pyz. Various optical parameters of these complexes are concise in Table 4.

4.5.2 Emission mechanism. The Jablonski diagram (Fig. 9) illustrates the potential energy transfer pathway within the synthesized complexes. Energy is transferred from T_1 of sensitizers to emissive levels of Sm(III) ion. For this transfer to occur efficiently, the T_1 level of the sensitizer must be appropriately positioned relative to the samarium emissive level. β-diketone ligands with C–F substituents have been shown to effectively lower the T_1 energy of sensitizers. T_1 energies for TTBD and pyz are 20 600 cm^{-1} and 26 820 cm^{-1}, respectively, while the emissive $^4G_{5/2}$ level of Sm(III) ion is located at 17 699 cm^{-1}.[41–43] Literature reports indicate that an ideal energy gap (ΔE) between 2000 and 5000 cm^{-1} between T_1 state of ligand and the emitting level of metal ion promotes optimal energy transfer.[44] Here, ΔE values are 2901 cm^{-1} for TTBD and 9121 cm^{-1} for pyz. Triplet state energies of pyz, TTBD and $^4G_{5/2}$ level of Sm(III) have been enlisted in Table 5 along with their energy gaps (ΔE). According to Dexter's energy transfer theory,[45] extremely large gaps hinder transfer efficiency due to insufficient spectral overlap, whereas too small a gap can result in back-transfer of energy from Ln(III) ion to ligand, thus weakening the luminescence. Despite these considerations, the observed strong emission signals indicate that the chosen sensitizers possess suitably aligned triplet states to facilitate efficient sensitization of Sm(III) ion. However, recent studies have suggested that sensitization may also occur *via* singlet excited states under certain conditions and therefore both excited states may contribute to the overall energy transfer process.

A comparison of the emission intensities among the solution phase complexes shows the following trend: SmD > SmM > SmA. The weaker emission seen in SmM is primarily due to the limited energy transfer pathway. It occurs effectively only between T_1 of TTBD and emitting level of Sm(III), with insufficient overlap from the pyz moiety, as confirmed by a large ΔE. This demonstrates that TTBD is the main contributor to sensitizing the metal ion. As SmD contains more TTBD groups, it emits more strongly than SmM. In contrast, SmA shows the least emission, attributed to the absence of a secondary ligand. Furthermore, water molecules coordinating the Sm(III) ion further quench the emission through non-radiative vibrational decay. The analysis of the individual emission bands (Fig. 10) indicates that the dominant contribution to the overall emission color arises from the $^4G_{5/2} \rightarrow {}^6H_{7/2}$ transition, while the $^4G_{5/2} \rightarrow {}^6H_{9/2}$ transition enhances the red component of the emission. The combined contributions of these transitions lead to the characteristic orange-red luminescence observed for the Sm(III) complexes.

4.5.3 Branching ratio. 'Relative distribution of emissions' among various peaks in luminescent Ln(III) complexes is a critical parameter affecting the overall efficiency of emission pathway. This aspect is particularly valuable for laser design, as this indicates the feasibility of achieving stimulated emission from specific electronic transitions.[46] The contribution of each individual transition in Sm(III) complexes can be quantitatively assessed through branching ratios, which are calculated using eqn (3).[47]

$$\beta = \frac{A_{\psi_J - \psi_{J'}}}{\sum A_{\psi_J - \psi_{J'}}} \times 100 \quad (2)$$

Here, $A_{\psi_J - \psi_{J'}}$ is integrated area under each peak observed in the PL spectra. Calculated branching ratio for Sm(III) complexes are

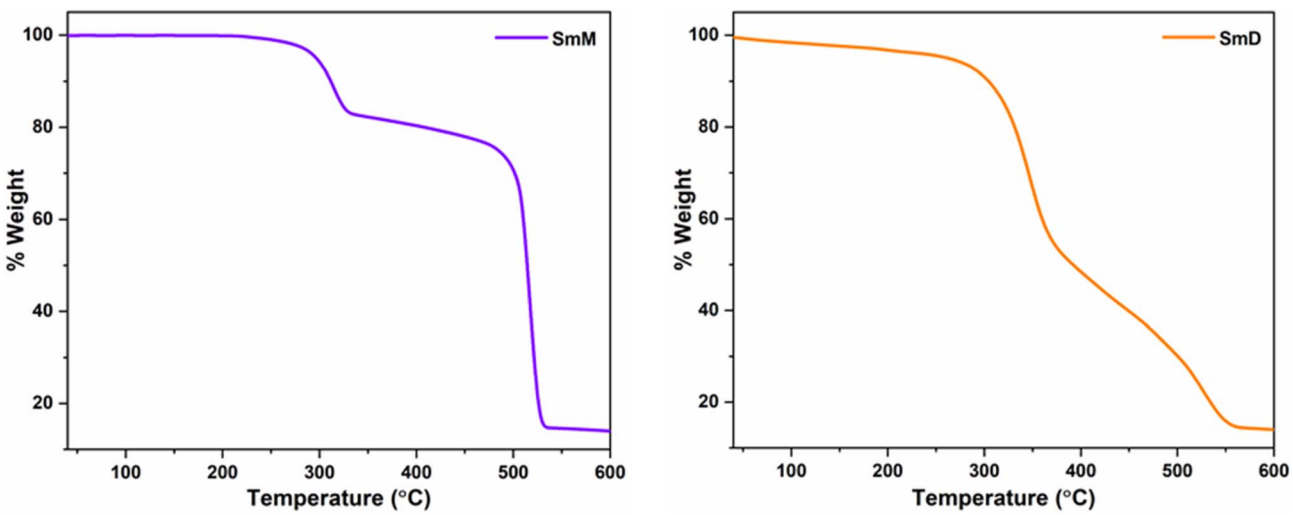

Fig. 13 TG profiles of SmM and SmD.

tabulated in Table 6. Notably, hypersensitive transitions *i.e.* $\Delta J = 2$ exhibit branching ratios nearing ~67%, highlighting their promising applicability in laser diode technologies.

4.5.4 Decay time. The emission decay lifetime plays an essential role in real-world application of luminescent practices, including FRET (Fluorescence Resonance Energy Transfer). Lifetimes of the prepared complexes were calculated *via* time-resolved luminescence spectroscopy at their respective λ_{ex} and λ_{em}. Luminescence lifetimes of prepared complexes are provided in Table 4, with their luminescence decay curves and corresponding fits for the $^4G_{5/2}$ energy level shown in Fig. 11, respectively. The emission decay curves are monoexponential, indicating a single luminescent site in the complexes. Relationship between emission intensity and decay lifetime is described by eqn (3).[48]

$$I(t) = I_0 e^{(-t/\tau)} \quad (3)$$

where I_0 being initial intensity and τ is lifetime. Luminescence lifetimes for SmA–SmD are 0.004, 0.058 and 0.063 ms, respectively. Lifetime for SmA is relatively short, possibly due to the existence of water moieties, that can increase non-radiative decay rates.[49] In SmM, metal ions are coordinatively saturated by three TTBD ligands (with low vibrational frequency C–F oscillators and quite appropriate T_1) and auxiliary pyz ligand. This coordinated environment shields the Sm(III) ions from external influences, leading to longer radiative emission lifetimes. Notably, present complexes SmM and SmD show longer $\Delta J = 2$ transition lifetimes compared to several reported Sm(III)-complexes, including analogous $[Sm(hfa)_3(phen)]$ (37 μs), $[Sm(hfaa)_3(impy)_2]$ (36 μs), $[Sm_2(tfaa)_6(\mu\text{-bpm})]$ (26 μs), $[Sm(EtDtc)_3(bipy)]$ (24.53 ± 0.01 μs), $[Sm(hfaa)_3(pz)_2]$ (39 μs), $[Sm(dbm)_3(phen)]$ (41 ± 2 μs),[50–55] $[Sm(tfaa)_3(phen)]$ (37.45 μs), $[Sm(tfaa)_3(bpy)]$ (37.14 μs) and $[Sm(hfa)_3(bpy)_2]$ (31.0 μs). The asymmetric nature of β-diketone (TTBD) probably led to this higher lifetime in prepared complexes.

4.5.5 Color modulation. CIE chromaticity coordinates (x and y) for SmA–SmD were determined from their PL spectra using CIE calculator. These calculated coordinates were then plotted on CIE 1931 chromaticity diagram (Fig. 12(a)). Complexes SmM and SmD exhibit similar orange-red emission coordinates, which can be attributed to their shared structural components namely the β-diketone ligand (TTBD) and the ancillary ligand (pyz). In contrast, a slight deviation in coordinate values is observed for SmA, likely due to the absence of the pyz in its coordination sphere along with the existence of water moieties, which reduces the energy transfer efficiency to Sm(III) ion. This is the same reason responsible for the appearance of the ligand based band. To further analyze the color characteristics, u' and v' coordinates were computed by inserting x and y values in the below mentioned equations (eqn (4)).[56]

$$u' = \frac{4x}{-2x + 12y + 3}, \quad v' = \frac{9y}{-2x + 12y + 3} \quad (4)$$

These values were subsequently plotted on CIE 1976 (u', v') chromaticity diagram (Fig. 12(b)), providing a more perceptually uniform representation of the emission color. To assess the visual quality of the emitted light, the correlated color temperature (CCT) was evaluated by McCamy's empirical formula (eqn (5))[57]

$$CCT = -437n^3 + 3601n^2 - 6861n + 5514.31 \quad (5)$$

where n is the reciprocal slope, given by $n = (x - x_e)/(y - y_e)$, with (x_e, y_e) being the chromaticity coordinates of the equal energy white point.[57] The CCT values, presented in Table 7, indicate that all complexes emit warm white light (CCT < 3500 K). Light sources with lower CCT values typically produce a warmer appearance, which is generally preferred for indoor lighting environments due to their comfortable visual perception. Therefore, the emission characteristics of the present Sm(III) complexes suggest their potential relevance as luminescent materials for warm-light generation in lighting and display applications.[58] Overall, these photophysical parameters collectively determine the emission quality and color characteristics of the complexes. The variation in coordination environment between the mononuclear and dinuclear complexes influences the ligand-to-metal energy transfer efficiency, which is reflected in the observed differences in emission intensity and photophysical parameters.

4.6 TG analysis

Thermal stability of Ln(III) complexes is a critical element influencing their applicability in Ln-based OLED devices.[59] Coordination interactions between the central ion and the spacer ligand play a crucial role, leading to significantly enhanced thermal stability in dinuclear systems.[60] Thermal behavior of prepared complexes was investigated over a temperature range of 40–600 °C using thermogravimetric analysis. Prior to TG analysis, the samples were dried to remove loosely bound solvent molecules. Thermograms of SmM and SmD are displayed in Fig. 13. For the precursor $[Sm(TTBD)_3 \cdot (H_2O)_2]$, the TG curve shows a weight loss between 80–120 °C due to removal of coordinated water molecules. However, in SmD, a small weight loss between 85–120 °C is observed which is attributed to the release of physically adsorbed moisture rather than coordinated solvent within the coordination sphere. On the contrary, TG curves of SmM does not show any mass loss till this temperature range, indicating that this complex is anhydrous. When comparing the thermal decomposition profiles of the complexes, it is observed that the complex with the pyz ligand displays a similar profile to the precursor, but with slightly higher thermal stability at higher temperatures.

TGA analysis of SmM shows that the complex remains stable up to 224 °C, with no detectable mass loss, indicating that all ligands are still coordinated to the Sm(III) ion. The first noticeable decomposition occurs at 224 °C and continues to 539 °C, during which the complex undergoes a total mass loss of 84.78%. Between 224 °C and 341 °C, around 17.01% of the mass is lost, corresponding to the release of two coordinated pyz ligands (theoretical/theor. value: 16.45%). From 341 °C to 539 °C, the removal of three TFPB ligands takes place (theoretical = 68.42%; calculated = 68.23%), ultimately yielding samarium

oxide (Sm_2O_3) as the thermal residue. Thermogram of SmD displays a 'small weight loss' (~3.2%) between 85–135 °C, due to elimination of residual moisture absorbed during transfer. First significant change occurs at 231 °C with a 5.3% weight loss, expressing the removal of pyz (theor. loss: 4.69%). The expulsion of TTBD starts before the 'complete removal of pyz.' Afterwards, the 'thermogram shows a continuous mass loss,' with ~39.97% of the mass removed by 561 °C, yielding samarium oxide (Sm_2O_3) as a thermal residue. Dinuclear complex shows higher thermal stability than its mononuclear conjugate. These TGA results indicate that the complexes possess reasonable thermal stability before the start of ligand decomposition, which is relevant for their potential use as luminescent materials.

5 Conclusions

In a one-pot reaction involving hydrated Sm(III) chlorides, TTBD and H_2O/pyrazine, with ammonium hydroxide solution, the complexes $[Sm(TTBD)_3(H_2O)_2]$ and $[Sm(TTBD)_3(pyz)_2]$, respectively are formed *in situ*. The 'pyrazine-bridged dinuclear samarium 1,3-diketonate complex of type $[(TTBD)_3Sm(\mu\text{-pyz})Sm(TTDB)_3]$ was formed *via* a two-step process. The formation of desired mononuclear complexes and the dinuclear complex is affirmed by CHN and IR analysis and validated by NMR results. Proton NMR spectra confirm symmetrical bridging of pyz to the two $Sm(TTBD)_3$ entities, as evidenced by a single sharp resonance in the 'aromatic region'. Coordination environment of three TTBD- and pyz ligands effectively shields the Sm(III) ions, providing protection from external factors and improving luminescence intensity and longer radiative lifetimes. Hypersensitive transition intensity of dinuclear complex (SmD) is twice that of the mononuclear SmA/SmM and the band shape resembles 'typical seven-coordinate β-diketonate complex.' Emission profile of SmD demonstrates a single peak for the $\Delta J = 2$ transition, indicating a single type of Sm(III) species, producing strong orange-red luminescence as validated by lifetime data. Coordination of metal ion with the bridging moiety enhances the thermal stability of dinuclear complex. Furthermore, electronic absorption data analyzed *via* Tauc's method, indicated semiconducting properties with optical band gaps near 3.3 eV. In other words, the dual features of visible emission and semiconducting behavior suggest their strong possibility for uses in optoelectronic and photonic gadgets. Although, the photophysical properties were investigated in solution, the observed luminescent behavior suggests that such complexes may be of interest for luminescent materials, although further studies in the solid state would be required to evaluate their potential applicability in optoelectronic devices.

Author contributions

Vandana Aggarwal: data curation, writing – original draft; Devender Singh: writing – review and editing and supervision; Swati Dalal: investigation; Shri Bhagwan: validation; Sumit Kumar: visualization; Rajender Singh Malik: resources; Parvin Kumar: formal analysis; Jayant Sindhu: software.

Conflicts of interest

No conflicts of interest to declare.

Data availability

The authors affirm that the information/data of this research article is available inside the article.

Supplementary information (SI): spectroscopic data. See DOI: https://doi.org/10.1039/d6ra00472e.

Acknowledgements

Vandana Aggarwal is thankful to UGC-New Delhi for providing SRF [221610012377].

References

1 Y. Hasegawa, Y. Kitagawa and S. Shoji, *Lanthanide-Based Wavelength Conversion Materials*. Springer, 2024, DOI: 10.1007/978-981-97-5636-0.
2 V. Aggarwal, D. Singh, A. Hooda, S. Malik, S. Dalal, S. Redhu, S. Kumar, R. S. Malik and P. Kumar, Comprehensive investigation of ternary dysprosium complexes for white light emission: Synthesis, spectroscopic and colorimetric analyses, *J. Lumin.*, 2024, **270**, 120555, DOI: 10.1016/j.jlumin.2024.120555.
3 D. Singh, S. Bhagwn, R. K. Saini, V. Nishal and I. Singh, Development in organic light-emitting materials and their potential applications, *Adv. Magn. Opt. Mater.*, 2016, **32**, 473–519, DOI: 10.1002/9781119241966.
4 V. Aggarwal, D. Singh, A. Hooda, K. Nehra, K. Jakhar, S. Kumar, R. S. Malik and P. Kumar, Synthesis and photoluminescent analyses of ternary terbium(III) Tris-β-diketonate complexes: A systematic exploration, *J. Mater. Sci.:Mater. Electron.*, 2024, **35**, 568, DOI: 10.1007/s10854-024-12314-z.
5 L. Arrué, J. Santoyo-Flores, N. Pizarro, X. Zarate, D. Páez-Hernández and E. Schott, The role played by structural and energy parameters of β-Diketones derivatives as antenna ligands in Eu(III) complexes, *Chem. Phys. Lett.*, 2021, **773**, 138600, DOI: 10.1016/j.cplett.2021.138600.
6 A. Hooda, D. Singh, K. Nehra, S. Dalal, V. Aggarwal, S. Kumar, R. S. Malik and P. Kumar, Preparation and optical studies of octacoordinated luminescent complexes of Dy(III) derived from fluorinated β-diketone and heteroaromatic neutral ligands, *Inorg. Chim. Acta*, 2023, **556**, 121674, DOI: 10.1016/j.ica.2023.121674.
7 K. Nehra, A. Dalal, A. Hooda, R. K. Saini, D. Singh and S. Kumar, Synthesis and photoluminescence characterization of the complexes of samarium dibenzoylmethanates with 1, 10-phenanthroline derivatives, *Polyhedron*, 2022, **217**, 115730, DOI: 10.1016/j.poly.2022.115730.

8 V. Aggarwal, D. Singh, K. Nehra, S. Dalal, S. Redhu, P. Kumar, S. Kumar and R. S. Malik, White light emission from a ternary dysprosium complex: Energy transfer and ligand-driven modulation, *Mater. Sci. Semicond. Process.*, 2025, **192**, 109427, DOI: 10.1016/j.mssp.2025.109427.

9 D. C. Zhong, Y. N. Gong, C. Zhang and T. B. Lu, Dinuclear metal synergistic catalysis for energy conversion, *Chem. Soc. Rev.*, 2023, **52**, 3170–3214, DOI: 10.1039/D2CS00368F.

10 K. Bernot, C. Daiguebonne, G. Calvez, Y. Suffren and O. Guillou, A journey in lanthanide coordination chemistry: from evaporable dimers to magnetic materials and luminescent devices, *Acc. Chem. Res.*, 2021, **54**, 427–440, DOI: 10.1021/acs.accounts.0c00684.

11 E. Kuzniak, D. Pinkowicz, J. Hooper, M. Srebro-Hooper, Ł. Hetmańczyk and R. Podgajny, Molecular Deformation, Charge Flow, and Spongelike Behavior in Anion–π $\{[M(CN)_4]^{2-};[HAT(CN)_6]\}\infty$ (M= Ni, Pd, Pt) Supramolecular Stacks, *Chem.–Eur. J.*, 2018, **24**, 16302–16314, DOI: 10.1002/chem.201802933.

12 D. Mara, F. Artizzu, P. F. Smet, A. M. Kaczmarek, K. Van Hecke and R. Van Deun, Vibrational Quenching in Near-Infrared Emitting Lanthanide Complexes: A Quantitative Experimental Study and Novel Insights, *Chem.–Eur. J.*, 2019, **25**, 15944–15956, DOI: 10.1002/chem.201904320.

13 L. Zapała, M. Kosińska, E. Woźnicka, Ł. Byczyński, E. Ciszkowicz, K. Lecka-Szlachta, W. Zapała and M. Chutkowski, Comparison of spectral and thermal properties and antibacterial activity of new binary and ternary complexes of Sm (III), Eu (III) and Gd (III) ions with N-phenylanthranilic acid and 1, 10-phenanthroline, *Thermochim. Acta*, 2019, **671**, 134–148, DOI: 10.1016/j.tca.2018.11.019.

14 D. Singh, K. Singh, S. Bhagwan, R. K. Saini, R. Srivastava and I. Singh, Preparation and photoluminescence enhancement in terbium (III) ternary complexes with β-diketone and monodentate auxiliary ligands, *Cogent Chem.*, 2016, **2**, 1134993, DOI: 10.1080/23312009.2015.1134993.

15 A. Hooda, A. Dalal, K. Nehra, D. Singh, S. Kumar, R. S. Malik and P. Kumar, Preparation and optical investigation of green luminescent ternary terbium complexes with aromatic β-diketone, *Chem. Phys. Lett.*, 2022, **794**, 139495, DOI: 10.1016/j.cplett.2022.139495.

16 A. Hooda, K. Nehra, A. Dalal, S. Singh, R. K. Saini, S. Kumar and D. Singh, Terbium complexes of an asymmetric β-diketone: preparation, photophysical and thermal investigation, *Inorg. Chim. Acta*, 2022, **536**, 120881, DOI: 10.1016/j.ica.2022.120881.

17 A. Hooda, K. Nehra, A. Dalal, S. Singh, S. Bhagwan, K. Jakhar and D. Singh, Preparation and photoluminescent analysis of Sm3+ complexes based on unsymmetrical conjugated chromophoric ligand, *J. Mater. Sci. Mater. Electron.*, 2022, **33**, 11132–11142, DOI: 10.1007/s10854-022-08089-w.

18 D. Singh, V. Tanwar, A. P. Simantilleke, B. Mari, P. S. Kadyan and I Singh, Rapid synthesis and enhancement in down conversion emission properties of BaAl2O4: Eu2+, RE3+ (RE3+= Y, Pr) nanophosphors, *J. Mater. Sci. Mater. Electron.*, 2016, **27**, 2260–2266, DOI: 10.1007/s10854-015-4020-1.

19 G. Li, D. Zhu, X. Wang, Z. Su and M. R. Bryce, Dinuclear metal complexes: multifunctional properties and applications, *Chem. Soc. Rev.*, 2020, **49**, 765–838, DOI: 10.1039/C8CS00660A.

20 A. Dalal, K. Nehra, A. Hooda, D. Singh, J. Dhankhar and S. Kumar, Fluorinated β-diketone-based Sm (III) complexes: spectroscopic and optoelectronic characteristics, *Luminescence*, 2022, **37**, 1328–1334, DOI: 10.1002/bio.4300.

21 A. Dalal, K. Nehra, A. Hooda, S. Singh, S. Bhagwan, D. Singh and S. Kumar, 2, 2′-Bipyridine based fluorinated β-Diketonate Eu (III) complexes as red emitter for display applications, *Inorg. Chem. Commun.*, 2022, **140**, 109399, DOI: 10.1016/j.inoche.2022.109399.

22 V. Aggarwal, D. Singh, S. Redhu, S. Malik, S. Dalal, S. Kumar, R. S. Malik, P. Kumar and J. Sindhu, Design and photophysical characterization of dinuclear lanthanide complexes incorporating spacer ligands along with their mononuclear analogues: A comparative study, *Opt. Mater.*, 2024, **155**, 115833, DOI: 10.1016/j.optmat.2024.115833.

23 A. Hooda, D. Singh, A. Dalal, K. Nehra, S. Kumar, R. S. Malik, H. Sehrawat and P. Kumar, N-donor auxiliary ligand-based terbium (III) β-diketonates: Preparation and photophysical studies, *J. Lumin.*, 2023, **258**, 119828, DOI: 10.1016/j.jlumin.2023.119828.

24 N. Ghosh, A. Bandyopadhyay, S. Roy, G. Saha and J. A. Mondal, Unified view of the hydrogen-bond structure of water in the hydration shell of metal ions (Li^+, Mg^{2+}, La^{3+}, Dy^{3+}) as observed in the entire 100–3800 cm^{-1} regions, *J. Mol. Liq.*, 2023, **389**, 122927, DOI: 10.1016/j.molliq.2023.122927.

25 V. Aggarwal, D. Singh, S. Bhagwan, R. K. Saini, K. Jakhar, R. S. Malik, P. Kumar and J. Sindhu, Exploring the influence of emissive centers in mono and dinuclear europium(III) complexes for advance lighting applications: Synthesis, characterization and computational modeling, *J. Mol. Struct.*, 2025, **1324**, 140841, DOI: 10.1016/j.molstruc.2024.140841.

26 K. Nehra, A. Dalal, A. Hooda, K. Jakhar, D. Singh and S. Kumar, Preparation, optoelectronic and spectroscopic analysis of fluorinated heteroleptic samarium complexes for display applications, *Inorg. Chim. Acta*, 2022, **537**, 120958, DOI: 10.1016/j.ica.2022.120958.

27 D. Parker, E. A. Suturina, I. Kuprov and N. F. Chilton, How the ligand field in lanthanide coordination complexes determines magnetic susceptibility anisotropy, paramagnetic NMR shift, and relaxation behavior, *Acc. Chem. Res.*, 2020, **53**, 1520–1534, DOI: 10.1021/acs.accounts.0c00275.

28 A. Hooda, D. Singh, K. Nehra, A. Dalal, S. Kumar, R. S. Malik, V. Siwach and P. Kumar, Photoluminescent Sm(III) diketonates with 1,10-phenanthroline derivatives: electrochemical and optoelectronic study, *J. Mater. Sci.:Mater. Electron.*, 2023, **34**, 1504, DOI: 10.1007/s10854-023-10899-5.

29 D. Singh, S. Bhagwan, A. Dalal, K. Nehra, K. Singh, A. Simantilleke, S. Kumar and I. Singh, Intense red luminescent materials of ternary Eu^{3+} complexes of oxide ligands for electroluminescent display devices, *Optik*, 2020, **208**, 164111, DOI: 10.1016/j.ijleo.2019.164111.

30 P. R. Jubu, O. S. Obaseki, F. K. Yam, S. M. Stephen, A. A. Avaa, A. A. McAsule, Y. Yusof and D. A. Otor, Influence of the secondary absorption and the vertical axis scale of the Tauc's plot on optical bandgap energy, *J. Opt.*, 2023, **52**, 1426–1435, DOI: 10.1007/s12596-022-00961-6.

31 P. Kumar, V. Gulia and A. G. Vedeshwar, Residual stress dependant anisotropic band gap of various (hkl) oriented BaI_2 films, *J. Appl. Phys.*, 2013, **114**, 193511, DOI: 10.1063/1.4832437.

32 S. Redhu, D. Singh, A. Hooda, S. Malik, V. Aggarwal, S. Dalal, S. Kumar, R. S. Malik and P. Kumar, Synthesis, characterization and luminescent properties of N-donor based samarium-tris-β-diketonate: Tuning optoelectronic characteristics for displays applications, *J. Mol. Struct.*, 2024, **1308**, 138056, DOI: 10.1016/j.molstruc.2024.138056.

33 K. Nehra, A. Dalal, A. Hooda, S. Bhagwan, R. K. Saini, B. Mari, S. Kumar and D. Singh, Lanthanides β-diketonate complexes as energy-efficient emissive materials: A review, *J. Mol. Struct.*, 2022, **1249**, 131531, DOI: 10.1016/j.molstruc.2021.131531.

34 K. Nehra, A. Dalal, A. Hooda, S. Singh, D. Singh, S. Kumar, R. S. Malik, R. Kumar and P. Kumar, Red luminous Eu (III) complexes: Preparation, spectral, optical and theoretical evaluation, *Inorg. Chim. Acta.*, 2022, **539**, 121007, DOI: 10.1016/j.ica.2022.121007.

35 M. B. Coban, A. Amjad, M. Aygun and H. Kara, Sensitization of HoIII and SmIII luminescence by efficient energy transfer from antenna ligands: Magnetic, visible and NIR photoluminescence properties of GdIII, HoIII and SmIII coordination polymers, *Inorg. Chim. Acta*, 2017, **455**, 25–33, DOI: 10.1016/j.ica.2016.10.010.

36 A. O. Sarıoğlu, Ş. P. Yalçın, Ü. Ceylan, M. Aygün, H. Kırpık and M. Sönmez, Photoluminescence properties of samarium(III)-based complexes: Synthesis, characterization and single crystal X-ray, *J. Lumin.*, 2020, **227**, 117537, DOI: 10.1016/j.jlumin.2020.117537.

37 V. Aggarwal, D. Singh, A. Hooda, K. Nehra, S. Redhu, S. Kumar, R. S. Malik and P. Kumar, Design and spectroscopic study of samarium complexes with tunable photoluminescent properties, *J. Mol. Struct.*, 2024, **1311**, 138315, DOI: 10.1016/j.molstruc.2024.138315.

38 A. Hooda, K. Nehra, A. Dalal, S. Singh, R. K. Saini, S. Kumar and D. Singh, Deep red emissive octacoordinated heteroleptic Sm (III) complexes: preparation and spectroscopic investigation, *J. Mol. Struct.*, 2022, **1260**, 132848, DOI: 10.1016/j.molstruc.2022.132848.

39 S. Redhu, D. Singh, A. Hooda, S. Malik, V. Aggarwal, S. Dalal, S. Kumar, R. S. Malik and P. Kumar, Photoluminescence tuning of terbium tris-1,1,1-trifluoro-5,5-dimethyl-2,4-hexanedione complexes: Synthesis, spectroscopic, thermal and electrochemical analyses, *J. Lumin.*, 2024, **271**, 120588, DOI: 10.1016/j.jlumin.2024.120588.

40 A. Kuznetsova, V. Matveevskaya, D. Pavlov, A. Yakunenkov and A. Potapov, Coordination polymers based on highly emissive ligands: Synthesis and functional properties, *Material*, 2020, **13**, 2699, DOI: 10.3390/ma13122699.

41 V. Aggarwal, D. Singh, S. Malik, S. Redhu, S. Kumar, R. S. Malik, P. Kumar and J. Sindhu, Tailoring photoluminescence in Sm(III) β-Diketonates: Impact of Heteroaryl substitution on optical and electronic behavior, *Polyhedron*, 2026, **291**, 118088, DOI: 10.1016/j.poly.2026.118088.

42 K. Remmers, R. G. Satink, G. von Helden, H. Piest, G. Meijer and W. L. Meerts, Gas-phase infrared spectroscopy on the lowest triplet state of the pyrazine–argon complex, *Chem. Phys. Lett.*, 2000, **317**, 197–202, DOI: 10.1016/S0009-2614(99)01387-1.

43 A. Dalal, K. Nehra, A. Hooda, S. Singh, D. Singh, S. Kumar, R. S. Malik and P. Kumar, Preparation, spectroscopic and thermal investigation of fluorinated Sm(III) β-diketonates with bidentate N donor ligands, *Chem. Phys. Lett.*, 2022, **800**, 139672, DOI: 10.1016/j.cplett.2022.139672.

44 K. Nehra, A. Dalal, A. Hooda, S. Singh, D. Singh, S. Kumar, R. S. Malik, R. Kumar and P. Kumar, Red luminous Eu (III) complexes: Preparation, spectral, optical and theoretical evaluation, *Inorg. Chim. Acta*, 2022, **539**, 121007, DOI: 10.1016/j.ica.2022.121007.

45 A. Dalal, A. Hooda, K. Nehra, D. Singh, S. Kumar, R. S. Malik and P. Kumar, Effect of substituted 2, 2′-bipyridine derivatives on luminescence characteristics of green emissive terbium complexes: Spectroscopic and optical analysis, *J. Mol. Struct.*, 2022, **1265**, 133343, DOI: 10.1016/j.molstruc.2022.133343.

46 Y. Hasegawa, Y. Wada and S. Yanagida, Strategies for the design of luminescent lanthanide(III) complexes and their photonic applications, *J. Photochem. Photobiol., C*, 2004, **5**, 183–202, DOI: 10.1016/j.jphotochemrev.2004.10.003.

47 S. Dalal, D. Singh, A. Dalal, A. Hooda, S. Kumar, R. S. Malik, P. Kumar and J. Sindhu, Green emissive Tb(III) complexes based on photosensitizing antenna: Synthesis and optoelectronic analysis, *Mater. Sci. Semicond. Process.*, 2024, **177**, 108370, DOI: 10.1016/j.mssp.2024.108370.

48 A. Dalal, K. Nehra, A. Hooda, S. Singh, D. Singh and S. Kumar, Synthesis, optoelectronic and photoluminescent characterizations of green luminous heteroleptic ternary terbium complexes, *J. Fluoresc.*, 2022, **32**, 1019–1029, DOI: 10.1007/s10895-022-02920-7.

49 S. Malik, K. Jakhar, D. Singh, S. Dalal, A. Hooda, K. Nehra, S. Kumar, R. S. Malik and P. Kumar, Exploring the role of neutral ligands in modulating the photoluminescence of samarium complexes with 1, 1, 1, 5, 5, 5-hexafluoro-2, 4-pentanedione, *Luminescence*, 2024, **39**, e4810, DOI: 10.1002/bio.4810.

50 H. Kawai, C. Zhao, S. Tsuruoka, T. Yoshida, Y. Hasegawa and T. Kawai, Emission properties of Sm(III) complexes having remarkably deep-red emission band, *J. Alloys Compd.*, 2009, **488**, 612–614, DOI: 10.1016/j.jallcom.2008.09.091.

51 W. A. Dar, A. B. Ganaie and K. Iftikhar, Synthesis and photoluminescence study of two new complexes

[Sm(hfaa)$_3$(impy)$_2$] and [Eu(hfaa)$_3$(impy)$_2$] and their PMMA based hybrid films, *J. Lumin.*, 2018, **202**, 438–449, DOI: 10.1016/j.jlumin.2018.05.032.

52 D. Singh, S. Bhagwan, V. Tanwar and R. K. Saini, Synthesis and optical characterization of color-tunable heterocyclic ligand based beryllium (II) complexes for white lighting applications, *Mater. Des.*, 2016, **100**, 245–253, DOI: 10.1016/j.matdes.2016.03.118.

53 X. Y. Chen, M. P. Jensen and G. K. Liu, Analysis of energy level structure and excited-state dynamics in a Sm(III) complex with soft-donor ligands: Sm(Et$_2$Dtc)$_3$(bipy), *J. Phys. Chem. B*, 2005, **109**, 13991–13999, DOI: 10.1021/jp0516700.

54 Z. Ahmed, W. Ahmed Dar and K. Iftikhar, Synthesis and luminescence study of a highly volatile Sm(III) complex, *Inorg. Chim. Acta*, 2012, **392**, 446–453, DOI: 10.1016/j.ica.2012.05.025.

55 J. M. Stanley, C. K. Chan, X. Yang, R. A. Jones and B. J. Holliday, Synthesis, X-ray crystal structure and photophysical properties of tris(dibenzoylmethanido)(1,10-phenanthroline) samarium(III), *Polyhedron*, 2010, **29**, 2511–2515, DOI: 10.1016/j.poly.2010.05.020.

56 P. Kumar, D. Singh, S. Kadyan, H. Kumar and R. Kumar, Cool green-emissive $Y_2Si_2O_7$:Tb^{3+} nanophosphor: auto-combustion synthesis and structural and photoluminescence characteristics with good thermal stability for lighting applications, *RSC Adv.*, 2024, **14**, 16560–16573, DOI: 10.1039/D4RA02571G.

57 R. Malik, K. Ray and S. Mazumdar, A low-cost, wide-range, CCT-tunable, variable-illuminance LED lighting system, *Leukos*, 2020, **16**, 157–176, DOI: 10.1080/15502724.2018.1541747.

58 G. Ozenen, *Architectural Interior Lighting*. Springer, 2023, DOI: 10.1007/978-3-031-49695-0.

59 A. Dalal, K. Nehra, A. Hooda, D. Singh, P. Kumar, S. Kumar, R. S. Malik and B. Rathi, Luminous lanthanide diketonates: Review on synthesis and optoelectronic characterizations, *Inorganica Chim. Acta*, 2023, **550**, 121406, DOI: 10.1016/j.ica.2023.121406.

60 E. Berti, A. Caneschi, C. Daiguebonne, P. Dapporto, M. Formica, V. Fusi, L. Giorgi, A. Guerri, M. Micheloni, P. Paoli and R. Pontellini, Ni (II), Cu (II), and Zn (II) Dinuclear Metal Complexes with an Aza−Phenolic Ligand: Crystal Structures, Magnetic Properties, and Solution Studies, *Inorg. Chem.*, 2003, **42**, 348–357, DOI: 10.1021/ic0204070.